

# DATA ASSIMILATION IN THE LOW NOISE, ACCURATE OBSERVATION REGIME WITH APPLICATION TO THE KUROSHIO CURRENT

ERIC VANDEN-EIJNDEN AND JONATHAN Q. WEARE

**ABSTRACT.** On-line data assimilation techniques such as ensemble Kalman filters and particle filters tend to loose accuracy dramatically when presented with an unlikely observation. Such an observation may be caused by an unusually large measurement error or reflect a rare fluctuation in the dynamics of the system. Over a long enough span of time it becomes likely that one or several of these events will occur. In some cases they are signatures of the most interesting features of the underlying system and their prediction becomes the primary focus of the data assimilation procedure. The Kuroshio current that runs along the eastern coast of Japan is an example of just such a system. It undergoes infrequent but dramatic changes of state between a small meander during which the current remains close to the coast of Japan, and a large meander during which the current bulges away from the coast. Because of the important role that the Kuroshio plays in distributing heat and salinity in the surrounding region, prediction of these transitions is of acute interest. Here we propose several data assimilation strategies capable of efficiently handling rare events such as the transitions of the Kuroshio current in situations where both the stochastic forcing on the system and the observational noise are small. In this regime, large deviation theory can be used to understand why standard filtering methods fail and guide the design of the more effective data assimilation techniques suggested here. These techniques are tested on the Kuroshio and shown to perform much better than standard filtering methods.

## 1. INTRODUCTION

The assimilation of noisy observations into a model to improve its predictive capabilities is a recurring challenge in many applications. Examples include weather prediction and forecasting, robot tracking, stochastic volatility estimation, image analysis, etc. (see [8]). In these applications and many others one is interested in predicting how the system evolves in time given a model for its dynamics and sequentially available, incomplete observations of its state. For practical reasons it is desirable to assimilate the observations in real time (“on-line”) via a recursive algorithm that requires only the latest observation together with the previous estimate of the system’s state. In the simplest case of Gaussian (i.e. linear) evolution and Gaussian observations, a solution to this problem is given by the Kalman filter (see [18]) and extensions thereof (see [11, 25, 16]), which predict how the mean and the variance of the system’s state evolve given the observations. For problems with significantly non-Gaussian features, Kalman filters are unsuitable (see [2, 21, 20] and the numerical results in Section 5.5.1), and particle filters, first suggested in [14] and [19], can be used instead. Particle filters, also known as sequential Monte Carlo methods, are recursive assimilation algorithms that predict how the posterior distribution of the system’s state evolves given the observations. They can in principle be applied to general, nonlinear, non-Gaussian situations, though they can be impractical in high dimensional problems (see [4]). An additional problem that both Kalman filters and particle filters share is that they tend to fail when the system undergoes occasional, unusually large transitions revealed by an observation that is inconsistent with the predictive distribution of the system’s state. Over long periods of time such transitions are inevitable and in some systems they are precisely the events of main interest. Our aim here is to develop filtering techniques capable of handling such situations.

An interesting example of a system exhibiting very occasional but interesting transitions that present significant challenges to standard data assimilation strategies is the Kuroshio current running along the eastern coast of Japan. The Kuroshio current exhibits transitions between a small meander during which the current remains close to the coast of Japan, and a large meander during which the current bulges away from the coast (see Figures 1 and 2). The Kuroshio’s central role in distributing heat and salinity in the surrounding region has led to many studies of its bimodal behavior beginning with a study by Yoshida in 1961 (see [34]). The meanders typically persist for 5-10 years, while the transitions between them occur in only a few months. Here we focus on a simple model qualitatively capturing the bimodal behavior of the Kuroshio as a test bed for our new filtering strategies, and we show that they remain effective in a regime where standard filtering techniques fail dramatically. Our general statements and results apply to systems

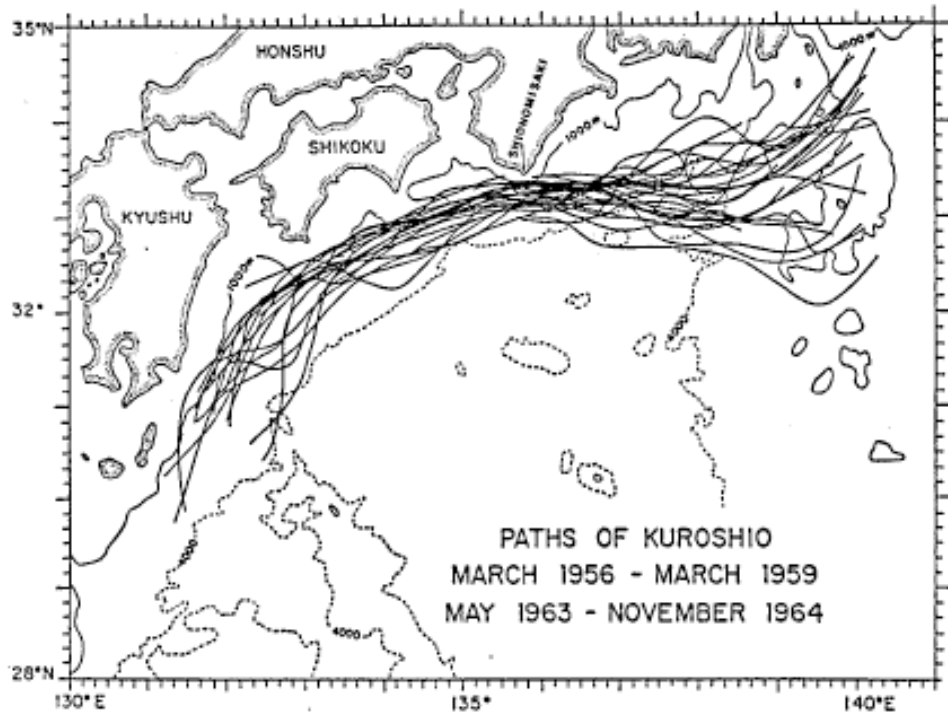


FIGURE 1. Paths in the small meander state. (Reproduced from [26]. Originally adapted from [28].)

exhibiting less dramatic and less interesting rare events, as these also occur eventually and lead to a loss of accuracy in standard filtering techniques.

We shall focus primarily on situations where the system is forced by a small stochastic term and the observational noise is small, as this regime is the most challenging for standard filters. In this low noise, accurate observation regime, the behavior of rare events such as the transitions of the Kuroshio can be understood within the framework of large deviations theory (see [9, 10, 13, 30]). This theory is built on the key observation that, when a rare event occurs, it typically does so in a predictable way by the most likely path possible. While the event is rare and the likelihood of observing this path is small, the likelihood of observing any other path is much smaller. The identification of the most likely path is at the core of a family of data assimilation techniques, called variational methods (e.g. 3DVar and 4DVar), that do effectively handle non-linearities in the underlying system (see [27]). These methods do not involve any sampling. Instead they find the solution to a large optimization problem which gives either the most likely current state of the system given the observations or the most likely path of the system over several observational windows. Unfortunately these methods provide only an estimate of the most likely trajectory of the system given the observations and do not provide further information about the distribution of the system. Moreover, they are not directly suitable for on-line data assimilation.

Several authors have suggested combining sampling methods with variational methods (see e.g. [33] and references therein). The framework we suggest in this paper follows this line of thought and naturally leads to hybrid data assimilation techniques sharing characteristics of both sampling based filters and variational methods. More specifically, we use information about the most likely path for the event to do importance sampling within the particle filters. This approach not only leads to filters that remain accurate in the presence of rare events, but it also allows one to predict the behavior of new and existing data assimilation schemes. We demonstrate that, in the small noise regime that is our focus, standard schemes can be expected to behave very poorly when the underlying system undergoes a rare large change in its state. The framework and methods suggested here should also shed some light on interesting and related methods such as path sampling based techniques (see [1, 2, 32]) and implicit sampling (see [7, 6]).

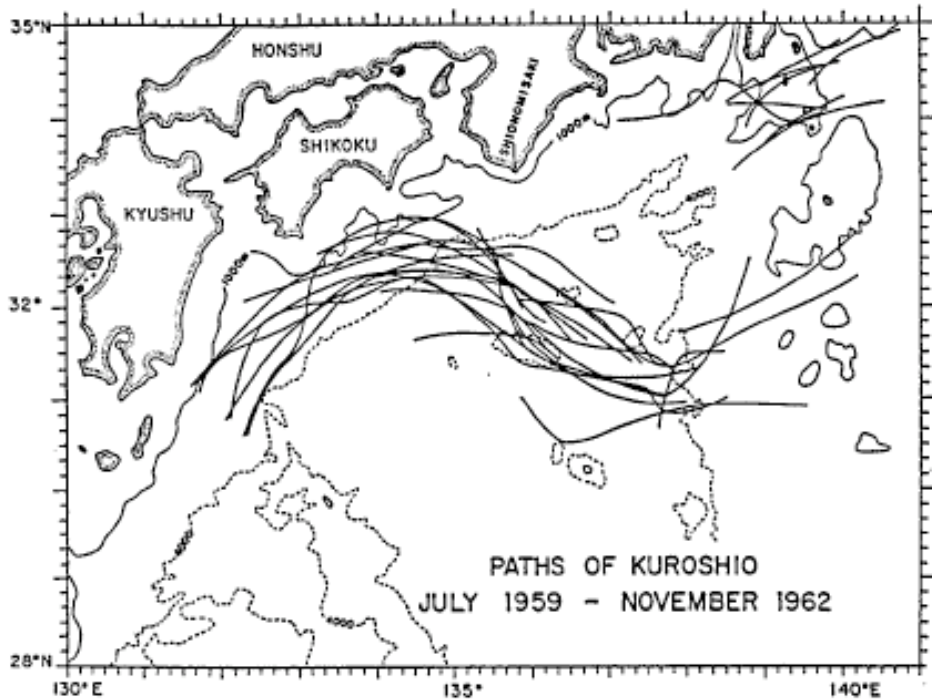


FIGURE 2. Paths in the large meander state. (Reproduced from [26]. Originally adapted from [28].)

The remainder of this paper is organized as follows. In Section 2 we describe the filtering problem along with the most basic versions of the Kalman filter (Section 2.2.1) and a particle filter (Section 2.2.2). In Section 3 we discuss the difficulties that these filters encounter in the small noise, accurate observation regime. In Section 4, we propose several hybrid sampling strategies. Section 5 presents the results of our numerical experiments on a simple model of the Kuroshio. Some conclusions are given in Section 6. Finally, in Appendices A and B we give details of some aspects of the numerical implementation of our algorithms.

## 2. STANDARD FILTERING METHODS

The goal of any discrete-time filtering algorithm is to approximately reconstruct the trajectory of some time-dependent process  $X(t)$  from observations  $H_1, H_2, \dots$  taken at a discrete set of times  $t_1, t_2, \dots$ . The observations are typically incomplete and made with measurement error, i.e. they are of the form

$$H_n = G(X(t_n))$$

where the  $G(x)$  is a random function modeling noisy observations of some part of the system. We will assume that, conditioned on  $X(t_n) = x_n$ , the observations,  $H_n$ , admit a probability density function

$$p(h_n|x_n)$$

where here and below we follow standard practice and label random variables with upper case letters (e.g.  $X(t_n)$ ,  $H_n$ , etc.) and the values assumed by those random numbers with lower case letters (e.g.  $x_n$ ,  $h_n$ , etc.). The underlying process  $X(t)$  should be considered “hidden” and revealed only through the observations. Ideally one would like to calculate modes and moments of the conditional distribution of the hidden signal  $X(t)$  given these observations. For example, one may wish to approximate the expectation of  $f(X(t_n))$  conditional on  $H_1 = h_1, \dots, H_n = h_n$ ,

$$(1) \quad \mathbf{E} [f(X(t_n)) | h_1, \dots, h_n]$$

When the underlying process  $X(t)$  is Markovian there are several recursive approaches to the approximation of quantities such as (1). These methods are based on the relationship

$$(2) \quad p(x_n | h_1, \dots, h_n) = \frac{p(h_n | x_n) \int p(x_n | x_{n-1}) p(x_{n-1} | h_1, \dots, h_{n-1}) dx_{n-1}}{p(h_n | h_1, \dots, h_{n-1})}$$

which follows from the Markov property of  $X(t)$  and Bayes' Formula. Here  $p(x_n | h_1, \dots, h_n)$ , denotes the probability density function of  $X(t_n)$  conditional on  $H_1 = h_1, \dots, H_n = h_n$ , and will be referred to as the posterior density, and  $p(x_n | x_{n-1})$ , denotes the density of  $X(t_n)$  conditional on  $X(t_{n-1}) = x_{n-1}$  and will be referred to as the predictive density. The interpretation of equation (2) is simple: it states that to obtain the posterior density at time  $t_n$  from the posterior density at time  $t_{n-1}$  one can first integrate the system from time  $t_{n-1}$  to time  $t_n$  with initial conditions drawn from the posterior density at time  $t_{n-1}$  and then discount the resulting samples by a weight proportional to  $p(h_n | x_n)$ . In fact, if  $X(t_{n-1})$  is assumed to be drawn from  $p(x_{n-1} | h_1, \dots, h_{n-1})$ , then

$$\mathbf{E}[f(X(t_n)) | h_1, \dots, h_n] = \frac{\mathbf{E}[f(X(t_n)) p(h_n | X(t_n))]}{\mathbf{E}[p(h_n | X(t_n))]}$$

There are several methods by which one might hope to approximately carry out the recursion (2). Perhaps the most obvious approach is to simply compute the integral using some quadrature scheme. This approach suffers from two insurmountable difficulties. The first is that there is often no closed form expression for the predictive density  $p(x_n | x_{n-1})$ . The second is that numerical quadrature becomes computationally impractical in more than a few dimensions. Two popular approximation methods that have been applied successfully in various settings are Kalman and particle filters. The next two subsections briefly describe these two approaches.

**2.1. Kalman filter.** In the case that  $\log p(h_n | x_n)$  is a quadratic function of  $x_n$  and that both the initial density and the predictive density  $p(x_n | x_{n-1})$  are Gaussian (which is true if the evolution of  $X(t)$  is governed by a linear equation), it is easy to see from (2) that the posterior density  $p(x_n | h_1, \dots, h_n)$  is also Gaussian. In this case to completely describe the posterior density one needs only find formulas for its mean and variance, which are obtained by easy manipulations of  $p(h_n | x_n)$ ,  $p(x_n | x_{n-1})$ , and the initial density. In fact, from (2) one can derive recursive formulas for the mean and the variance of  $p(x_n | h_1, \dots, h_n)$ . The resulting recursive scheme is called the Kalman filter (see [18]).

There are several important derivatives of the Kalman filter. These methods use Gaussian approximations of the densities appearing in (2) ( $p(h_n | x_n)$ ,  $p(x_n | x_{n-1})$ , and the initial condition) and are accurate in regimes in which these densities are nearly Gaussian. A particularly effective variant, the ensemble Kalman filter (see [11]), proceeds from an estimate of the mean  $\hat{m}_{n-1}$  and covariance  $\hat{\Sigma}_{n-1}$  of  $p(x_{n-1} | h_1, \dots, h_{n-1})$  as follows

**Algorithm 1** (Basic ensemble Kalman filter).

- (1) Generate  $M$  independent Gaussian vectors,  $\{X_j(t_{n-1})\}_{j=1}^M$ , with mean  $\hat{m}_{n-1}$  and covariance  $\hat{\Sigma}_{n-1}$ .
- (2) For each  $j$ , evolve  $X_j(t_{n-1})$  from time  $t_{n-1}$  to time  $t_n$  to generate an independent sample  $\tilde{X}_j(t_n)$  from  $p(x_n | X_j(t_{n-1}))$ . Note that, in general, these samples are no longer Gaussian.
- (3) Compute the sample mean  $m_n$  and sample covariance  $\Sigma_n$  of  $\{\tilde{X}_j(t_n)\}_{j=1}^M$ .
- (4) Analytically compute the mean  $\hat{m}_n$  and covariance  $\hat{\Sigma}_n$  of the posterior Gaussian density

$$C^{-1} p(h_n | x_n) e^{-\frac{1}{2}(x_n - m_n)^\top \Sigma_n^{-1} (x_n - m_n)}.$$

where  $C$  is a normalization factor.

**2.2. Particle filter.** Particle filtering is a very general sequential importance sampling implementation of the recursion in (2) (see [14, 19, 23, 22, 8]). Assuming that one has samples approximately generated from the posterior density at time  $t_{n-1}$ , one first evolves the samples forward to time  $t_n$  (as in the ensemble Kalman filter). At this point one has samples approximately drawn from

$$p(x_n | h_1, \dots, h_{n-1}) = \int p(x_n | x_{n-1}) p(x_{n-1} | h_1, \dots, h_{n-1}) dx_{n-1}.$$

One then assigns to a sample at position  $x_n$  the importance weight  $p(h_n | x_n)$ , proportional to

$$\frac{p(x_n | h_1, \dots, h_n)}{p(x_n | h_1, \dots, h_{n-1})}$$

(the proportionality follows from (2)).

At the next observation time these steps are repeated. The sample weights from the previous observation time will be multiplied by weights corresponding to the new observation. Over several observation times this leads to highly degenerate weights and poor statistical properties of the resulting estimator. To avoid this problem the standard particle filter includes a simple resampling step. The full procedure is summarized in the following algorithm (see [14]):

**Algorithm 2** (Basic particle filter).

- (1) Begin with  $M$  weighted samples  $\{(X_j(t_{n-1}), W_j(t_{n-1}))\}_{j=1}^M$  of  $p(x_{n-1} | h_1, \dots, h_{n-1})$ .
- (2) For each  $j$ , evolve  $X_j(t_{n-1})$  from time  $t_{n-1}$  to time  $t_n$  to generate an independent sample  $\tilde{X}_j(t_n)$  from  $p(x_n | X_j(t_{n-1}))$ .
- (3) Evaluate the weights,

$$\tilde{W}_j(t_n) = p(h_n | \tilde{X}_j(t_n)) W_j(t_{n-1}).$$

- (4) Resample the particles if necessary to obtain a weighted ensemble  $\{(X_j(t_n), W_j(t_n))\}_{j=1}^M$  approximating  $p(x_n | h_1, \dots, h_n)$ .

### 3. THE SMALL NOISE ACCURATE OBSERVATION REGIME

Assume for the moment that in the particle filter, one resamples at each step so that  $W_j(t_n) = 1/M$ . Notice that Step 2 is identical in both Algorithms 1 and 2. At the end of Step 2 both the ensemble Kalman filter and the particle filter have generated an empirical density,

$$(3) \quad \frac{1}{M} \sum_{j=1}^M \delta(x_n - \tilde{X}_j(t_n))$$

approximating  $p(x_n | h_1, \dots, h_{n-1})$ . In the ensemble Kalman filter this empirical density is approximated by a Gaussian density allowing the information from the observation at time  $t_n$  to be incorporated analytically. The particle filter uses the importance weights to transform (3) into a weighted empirical density approximating  $p(x_n | h_1, \dots, h_n)$ .

The difficulty with both methods is that the empirical density (3) provides a very poor approximation of the tails of the density  $p(x_n | h_1, \dots, h_{n-1})$ . Of course most observations (i.e. values of  $h_n$ ) do not correspond to tail events of  $p(x_n | h_1, \dots, h_{n-1})$ . However, in many cases (e.g. the Kuroshio current), these tail events are precisely the most interesting features of the system and the events that one is primarily interested in capturing.

The practical consequence of these tail events is easily understood by considering the behavior of a particle filter on the Kuroshio current. Suppose that between two observations the hidden signal makes a transition from one meander to another. If at the time of the first observation, all samples are in the small meander, then at best only a few trajectories will make the transition to the large meander. Therefore at the time of the next observation, when new likelihood weights are calculated, almost all of the samples will receive negligible weight, resulting in an estimator with very low accuracy. As we will see in the next section the way to overcome this problem is to use rare event sampling methods to bias the evolution of samples toward regions of space where the observation weights are large. In order to introduce these methods, let us first formalize the discussion on rare events: indeed many methods have been proposed in the past to deal with these events (see [8, 7, 6]) but the issues they pose do not seem to have been identified precisely.

To this end consider the situation in which the dynamics are governed by the stochastic differential equation

$$(4) \quad \begin{aligned} \dot{X}(t) &= b(X(t)) + \sqrt{\epsilon} \sigma(X(t)) \dot{B}(t) \\ X(0) &= x_0 \end{aligned}$$

where  $\dot{B}$  is Gaussian white noise. Assume also that the observations admit a conditional density of the form

$$(5) \quad p(h_n | x_n) \propto e^{-\frac{1}{\epsilon} g(h_n, x_n)}.$$

In both equations  $\epsilon$  is a small parameter. In this setup both the stochastic forcing in the dynamics and the observation noise are small.

To make the case for rare event simulation tools in data assimilation problems we will focus on the particle filter. However, as our numerical tests will highlight, the difficulties presented by rare events are shared by the Kalman filter family of methods as well. Consider the assimilation of a single observation  $H_1 = h_1$  at time  $t_1$  starting from initial condition  $X(0) = x_0$ . In particular consider the weights  $\tilde{W}_j$  generated in Step 3 of Algorithm 2. When these weights are constant the samples  $\tilde{X}_j(t_1)$  generated in Step 2 are exactly samples from the posterior density  $p(x_1 | h_1)$ . The variation in the weights is a measure of the distance of the empirical density (3) from the posterior density. It is natural then to consider the behavior of the relative standard deviation of the weights,

$$(6) \quad \rho = \frac{\sqrt{\mathbf{E} \left[ \left( \tilde{W}_j - \mathbf{E} \left[ \tilde{W}_j | H_1 = h_1 \right] \right)^2 | H_1 = h_1 \right]}}{\mathbf{E} \left[ \tilde{W}_j | H_1 = h_1 \right]}.$$

It would be perfectly reasonable to omit the conditioning on  $H_1$  in the previous expression. However, we will be modifying the dynamics of our system between observations (here between time 0 and  $t_1$ ) based on the next observation (here at time  $t_1$ ) and therefore we must assume that the next observation is available. The weights at observation time  $t_1$  are identically distributed so the subscript  $j$  in the previous display can be ignored. Expression (6) can be rewritten as

$$(7) \quad \rho = \sqrt{R - 1}$$

where

$$(8) \quad R = \frac{\mathbf{E} [W_j^2]}{\mathbf{E} [W_j]^2} = \frac{\mathbf{E} \left[ e^{-\frac{2}{\epsilon} g(h_1, X(t_1))} \right]}{\mathbf{E} \left[ e^{-\frac{1}{\epsilon} g(h_1, X(t_1))} \right]^2}.$$

Note that  $R \geq 1$  since the expectation of the square of a random variable is always greater than the square of its expectation. If  $R = 1$  the statistical error vanishes completely. By dividing the number of samples by  $R - 1$  one obtains the so called effective sample size, a rule of thumb giving the number of unweighted samples that would be equivalent (in terms of statistical accuracy) to an ensemble of weighted samples (see for example [8]).

Let us estimate  $R$  in the present context. The Laplace Principle (see e.g. [9, 10, 30]) indicates that, under suitable assumptions,

$$(9) \quad \mathbf{E} \left[ e^{-\frac{1}{\epsilon} g(h_1, X(t_1))} \right] \asymp e^{-\gamma_1/\epsilon}$$

where two functions of  $\epsilon$  are asymptotically equivalent ( $\asymp$ ) if the ratio of their logarithms converges to 1 as  $\epsilon \rightarrow 0$ . The constant  $\gamma_1$  is given by the formula

$$\gamma_1 = \inf_{\varphi(0)=x_0} \{I(\varphi) + g(h_1, \varphi(t_1))\}$$

where the infimum is taken over all absolutely continuous functions,  $\varphi$ , from  $[0, t_1]$  into  $\mathbb{R}^d$  and

$$(10) \quad I(\varphi) = \int_0^{t_1} \frac{1}{2} |\sigma(\varphi(t))^{-1} (\dot{\varphi}(t) - b(\varphi(t)))|^2 dt.$$

In our context this simply says that in the small noise regime the posterior density is sharply peaked around the states that are most likely (in the small noise limit) given the observations.

Applying the Laplace Principle one more time we obtain

$$(11) \quad \mathbf{E} \left[ e^{-\frac{2}{\epsilon} g(h_1, X(t_1))} \right] \asymp e^{-\gamma_2/\epsilon}$$

where

$$\gamma_2 = \inf_{\varphi(0)=x_0} \{I(\varphi) + 2g(h_1, \varphi(t_1))\}.$$

Notice that

$$(12) \quad \gamma_2 = \inf_{\varphi(0)=x_0} \{I(\varphi) + 2g(h_1, \varphi(t_1))\} \leq \inf_{\varphi(0)=x_0} \{2I(\varphi) + 2g(h_1, \varphi(t_1))\} = 2\gamma_1.$$

In most cases the inequality in (12) is strict and inserting (9) and (11) in (8) implies that  $R$  increases exponentially as  $\epsilon \rightarrow 0$ :

$$R \asymp e^{\frac{2\gamma_1 - \gamma_2}{\epsilon}}.$$

In other words, the number of samples needed to maintain accuracy increases exponentially as  $\epsilon \rightarrow 0$ . This is the primary challenge posed by rare events.

Before closing this section we should remark that while the finite time horizon setting (finite  $t_1$ ) described here seems appropriate for designing on-line filtering methods, it is not the appropriate setting for studying the transition mechanism of the system itself. This transition has a natural time scale (which probably has nothing to do with the observation window  $t_1$ ) on which it occurs. Methods for analyzing such events can be found in [15].

#### 4. IMPORTANCE SAMPLING STRATEGIES

The difficulty discussed in the previous section can be remedied within the context of importance sampling as we now describe. Recall our assumption that the original dynamics of the system are governed by the stochastic differential equation (4)

$$\begin{aligned}\dot{X}(t) &= b(X(t)) + \sqrt{\epsilon} \sigma(X(t)) \dot{B}(t) \\ X(0) &= x_0\end{aligned}$$

We now modify these dynamics by adding an additional forcing term  $v(t, x)$  so that instead of evolving (4) we evolve

$$(13) \quad \begin{aligned}\dot{\hat{X}}(t) &= b(\hat{X}(t)) + \sigma(\hat{X}(t)) v(t, \hat{X}(t)) + \sqrt{\epsilon} \sigma(\hat{X}(t)) \dot{B}(t) \\ \hat{X}(0) &= x_0.\end{aligned}$$

Girsanov's Theorem (see e.g. [17]) tells us that, for reasonable choices of  $v$ , the ratio of the probability of a path over the interval  $[0, t]$  under the original dynamics to a path under the modified dynamics (13) is given by

$$\frac{d\mathbf{P}}{d\mathbf{Q}} = e^{-\frac{1}{\sqrt{\epsilon}} \int_0^t \langle v(s, \hat{X}(s)), dB(s) \rangle - \frac{1}{2\epsilon} \int_0^t |v(s, \hat{X}(s))|^2 ds}.$$

Thus we can compute any expectation with respect to the original dynamics by instead computing a weighted expectation over the modified dynamics, i.e.

$$\mathbf{E}[f(X)] = \int f(x) d\mathbf{P}(x) = \int f(\hat{x}) \frac{d\mathbf{P}}{d\mathbf{Q}}(\hat{x}) d\mathbf{Q}(\hat{x}) = \mathbf{E}\left[f(\hat{X}) \frac{d\mathbf{P}}{d\mathbf{Q}}(\hat{X})\right]$$

where in this formal expression  $\mathbf{P}$  is the measure of a path under the original dynamics and  $\mathbf{Q}$  is the measure of a path under the dynamics biased by  $v$ . In particular, Steps ii and iii of Algorithm 2 can be replaced by

- ii' For each  $j$ , generate an independent sample  $\hat{X}_j$  of the solution to the modified stochastic differential equation

$$\begin{aligned}\dot{\hat{X}}_j(t) &= b(\hat{X}_j(t)) + \sigma(\hat{X}_j(t)) v(t, \hat{X}_j(t)) + \sqrt{\epsilon} \sigma(\hat{X}_j(t)) \dot{B}_j(t), \quad t \in [t_{n-1}, t_n] \\ \hat{X}_j(t_{n-1}) &= X_j(t_{n-1}).\end{aligned}$$

and

- iii' Evaluate the weights,

$$\hat{W}_j = e^{-\frac{1}{\epsilon} g(h_n, \hat{X}_j(t_n))} Z_j W_j(t_{n-1})$$

where

$$Z_j = e^{-\frac{1}{\sqrt{\epsilon}} \int_{t_{n-1}}^{t_n} \langle v(s, \hat{X}_j(s)), dB_j(s) \rangle - \frac{1}{2\epsilon} \int_{t_{n-1}}^{t_n} |v(s, \hat{X}_j(s))|^2 ds}.$$

The question then becomes how to choose  $v$  in (13) so that the ratio between the variance of the new weights  $\hat{W}_j$  and their mean square remain small, and we avoid the problem discussed in the previous section. This question is discussed next.

4.1. **The single observation case.** Let us again briefly assume that the process  $X$  is observed only once at time  $t_1$  and that  $H_1 = h_1$ . Our goal is to choose the function  $v$  so that the relative standard deviation of the weights in Step iii' above is as small as possible. This is not a trivial task. To see what it entails, note that the relative standard deviation of the new weights is

$$\rho = \sqrt{R - 1}$$

where now (compare (8))

$$(14) \quad R = \frac{\mathbf{E} \left[ \left( e^{-\frac{1}{\epsilon} g(h_1, \hat{X}(t_1))} \frac{d\mathbf{P}}{d\mathbf{Q}} \right)^2 \right]}{\mathbf{E} \left[ e^{-\frac{1}{\epsilon} g(h_1, \hat{X}(t_1))} \frac{d\mathbf{P}}{d\mathbf{Q}} \right]^2}$$

$$(15) \quad = \frac{\mathbf{E} \left[ e^{-\frac{2}{\epsilon} g(h_1, \hat{X}(t_1)) - \frac{2}{\sqrt{\epsilon}} \int_0^{t_1} \langle v(s, \hat{X}(s)), dB(s) \rangle - \frac{1}{\epsilon} \int_0^{t_1} |v(s, \hat{X}(s))|^2 ds} \right]}{\mathbf{E} \left[ e^{-\frac{1}{\epsilon} g(h_1, X(t_1))} \right]^2}.$$

As we have explained before, to control the relative standard deviation of the weights one must control  $R$ . Interestingly, there is one choice of the biasing function  $v$  which results in no statistical error at all (i.e. such that  $R = 1$ ). This choice will turn out to be impractical. However it will be useful to keep this ‘‘gold standard’’ in mind as we consider more practical possibilities. Specifically, if we define

$$\Phi(t, x) = \mathbf{E}_{t,x} \left[ e^{-\frac{1}{\epsilon} g(h_1, X(t_1))} \right].$$

then it is possible to show that  $R = 1$  for every  $\epsilon$  if we take  $v = v^\epsilon$  with

$$(16) \quad v^\epsilon = -\epsilon \frac{\sigma^\top D_x \Phi^\epsilon}{\Phi^\epsilon}$$

In other words the process  $\hat{X}$  in (13) with  $v = v^\epsilon$  samples exactly from the density of  $X$  given the observation at time  $t_1$ . With this choice reweighting of the samples is unnecessary. The function  $\Phi^\epsilon$  satisfies the backward Kolmogorov equation

$$(17) \quad \partial_t \Phi^\epsilon + \langle b, D_x \Phi^\epsilon \rangle + \frac{\epsilon}{2} \text{tr} \sigma \sigma^\top D_x^2 \Phi^\epsilon = 0$$

with terminal condition  $\Phi(t_1, x) = e^{-\frac{1}{\epsilon} g(h_1, x)}$ . One could, therefore, attempt to discretize and solve the partial differential equation (17) to approximate (16). Unfortunately this strategy is impractical in more than a few dimensions. These ideas, however, can be modified and put to use in high dimensions. Notice that for each  $\epsilon > 0$  the function

$$(18) \quad G^\epsilon = -\epsilon \log \Phi^\epsilon$$

solves the second order Hamilton–Jacobi equation

$$(19) \quad -\partial_t G^\epsilon + \mathcal{H}(x, D_x G^\epsilon(t, x)) - \frac{\epsilon}{2} \text{tr} \sigma \sigma^\top D_x^2 G^\epsilon = 0$$

with terminal condition  $G^\epsilon(t_1, x) = g(h_1, x)$ , where

$$(20) \quad \mathcal{H}(x, p) = -\langle b(x), p \rangle + \frac{1}{2} |\sigma(x)^T p|^2.$$

In terms of  $G^\epsilon$ , the function  $v^\epsilon$  in (16) can be written

$$(21) \quad v^\epsilon = -\sigma^\top D_x G^\epsilon.$$

It is natural to replace  $G^\epsilon$  by its zero viscosity approximation  $G$ , i.e. by the viscosity solution to the first order Hamilton–Jacobi equation,

$$(22) \quad -\partial_t G + \mathcal{H}(x, D_x G(t, x)) = 0$$

with terminal condition  $G(t_1, x) = g(h_1, x)$ , and to use the function

$$(23) \quad v^0 = -\sigma^\top D_x G$$

in place of the choice in (16).



Direct solution of equation (22) is, again, not practical in more than a few dimensions. However, under mild assumptions (see [3, 12]), the solution of this equation has an optimal control representation

$$(24) \quad G(t, x) = \inf_{\varphi(t)=x} \{I_{t,t_1}(\varphi) + g(h_1, \varphi(t_1))\}$$

where the infimum is taken over all absolutely continuous functions on  $[t, t_1]$  and

$$I_{t,t_1}(\varphi) = \int_t^{t_1} \frac{1}{2} |\sigma(\varphi(s))^{-1} (\dot{\varphi}(s) - b(\varphi(s)))|^2 ds.$$

Notice that the constant  $\gamma_1$  in formula (9) is given by  $\gamma_1 = G(0, x_0)$ .

Assume that at any point  $(t, x)$  there is one minimal trajectory in (24), i.e. a trajectory  $\hat{\varphi}_{t,x}$  such that

$$(25) \quad G(t, x) = I_{t,t_1}(\hat{\varphi}_{t,x}) + g(h_1, \hat{\varphi}_{t,x}(t_1)).$$

Such a function  $\hat{\varphi}_{t,x}$  will be called the optimal control trajectory at  $(t, x)$ . It can be shown that

$$(26) \quad v^0(t, x) = \sigma^{-1}(x) \left( \dot{\hat{\varphi}}_{t,x}(t) - b(x) \right).$$

From expression (26) it is clear that the choice (23) requires that one solves the variational problem (24) at each point along the path of  $\hat{X}$  to find an optimal control trajectory at  $(s, \hat{X}(s))$  for each  $s \in [0, t_1]$ . Clearly, for problems in high dimensions solving (24) is not a trivial task and carrying this out ‘‘on-the-fly’’ could impose a significant computational burden. In fact, the cost of generating each sample trajectory of (13) with this choice of  $v$  is quadratic in  $t_1$ . However, when sampling sufficiently rare events this cost is more than made up for by the favorable statistical properties of the estimator corresponding to (23). The results in [29] imply that for  $v^0$  in (23),

$$\lim_{\epsilon \rightarrow 0} R = 1.$$

This should be contrasted with the case of the standard particle filter for which we recall that  $R$  grows exponentially with  $\epsilon^{-1}$ . Notwithstanding the results in [29], for the extremely high dimensional models common in climate and weather prediction it seems necessary to search for approximations which, while they will not match the statistical performance of the choice in (23), are less computationally burdensome.

In the following we suggest two possible choices for  $v$  that in our numerical experiments seem to be inexpensive and effective. Both methods require solving the optimization problem (24) at least once. The optimization problem (24) is highly structured and in our numerical experiments the cost of the each solution of (24) is roughly ten times the cost of simulating a single trajectory of the original system (4). In fact (24) is very similar to the variational problem at the heart of the 4DVar algorithm (see [27] and the references therein) and it is likely that algorithms already in use within the data assimilation community can be leveraged.

One natural further approximation of the optimal choice  $v^\epsilon$  is obtained by choosing a parameter  $0 < \tau \leq t_1$  and, for  $k \leq t_1/\tau$ , solving

$$(27) \quad \begin{aligned} \dot{\hat{X}}(t) &= b(\hat{X}(t)) + \sigma(\hat{X}(t)) v(t) + \sqrt{\epsilon} \sigma(\hat{X}(t)) \dot{B}(t) \\ v(t) &= v^0(t, \hat{\varphi}_{k\tau, \hat{X}(k\tau)}) \quad \text{for } t \in [k\tau, (k+1)\tau]. \end{aligned}$$

Over each interval of length  $\tau$  we have simply replaced the spatial variable in  $v^0$  by values along the optimal trajectory  $\hat{\varphi}$  starting from the position of the sample  $\hat{X}$  at the end of the previous length  $\tau$  interval. Note that on  $[k\tau, (k+1)\tau]$  we can write

$$v(t) = \sigma^{-1}(\hat{\varphi}_{k\tau, \hat{X}(k\tau)}(t)) \left( \dot{\hat{\varphi}}_{k\tau, \hat{X}(k\tau)}(t) - b(\hat{\varphi}_{k\tau, \hat{X}(k\tau)}(t)) \right).$$

For example, the choice  $\tau = t_1$  yields

$$v(t) = v^0(t, \hat{\varphi}_{0,x}(t)) = \sigma^{-1}(\hat{\varphi}_{0,x}(t)) \left( \dot{\hat{\varphi}}_{0,x}(t) - b(\hat{\varphi}_{0,x}(t)) \right).$$

**4.2. Some simple recursive schemes for the multiple observation case.** The picture that we have sketched changes slightly when assimilating multiple sequential observations. In general no recursive algorithm can completely avoid poor performance as  $\epsilon \rightarrow 0$ . To see this suppose that between each observation in Algorithm 2 (with Steps i i' and i i i') we use the biasing function  $v^\epsilon$ . In the single observation case the choice  $v^\epsilon$  led to perfect sampling. In the multiple observation case however, after assimilating the first observation we are forced to use some approximation of the posterior density at time  $t_1$  (an empirical approximation in the case of Algorithm 2). Unfortunately the states at time  $t_1$  that are most consistent with the observation at time  $t_2$  may be far into tail of the time  $t_1$  posterior density. Resolution in this tail will be very poor leading to large errors as  $\epsilon$  vanishes.

One solution to this problem is to go back to time  $t_0$  and choose a function  $v$  that incorporates the observations at both  $t_1$  and  $t_2$ . In principle the states at time  $t_1$  that are most relevant to any future observation (not just at  $t_2$ ) may lie in the tail of the time  $t_1$  posterior density and one might have to “backtrack” many observational steps each time a new observation arrives. Though potentially costly this backtracking is fairly easy to implement. However, our numerical results indicate that significant statistical improvements are possible without backtracking and we will not pursue the topic further here.

The first algorithm that we suggest is a simple adaptation of the biasing function in (27) to the particle filtering framework:

**Algorithm 3.**

- (1) Begin with  $M$  unweighted samples  $\{X_j(t_{n-1})\}_{j=1}^M$  approximately drawn from  $p(x_{n-1} | h_1, \dots, h_{n-1})$ .
- (2) For each  $j$  generate an independent sample  $\hat{X}_j$  of the solution to (27) on  $[t_{n-1}, t_n]$  starting from  $\hat{X}_j(t_{n-1})$ . Label the corresponding trajectory of  $v$  in (27) by  $v_j(t)$ ,  $t \in [t_{n-1}, t_n]$ .
- (3) Evaluate the weights,

$$\hat{W}_j = e^{-\frac{1}{\epsilon} g(h_n, \hat{X}_j(t_n))} Z_j W_j(t_{n-1})$$

where

$$Z_j = e^{-\frac{1}{\sqrt{\epsilon}} \int_{t_{n-1}}^{t_n} \langle v_j(s), dB_j(s) \rangle - \frac{1}{2\epsilon} \int_{t_{n-1}}^{t_n} |v_j(s)|^2 ds}$$

- (4) Resample the particles if necessary to obtain a weighted ensemble  $\{(X_j(t_n), W_j(t_n))\}_1^M$  approximating  $p(x_n | h_1, \dots, h_n)$ .

While fairly simple and, in our tests, effective, Algorithm 3 still requires that one solve the optimization problem (24) once for each particle at each observation. In practice this may not be necessary. The following *ad-hoc* algorithm solves the optimization problem (24) only once at each step. The reader should note the similarity with the ensemble Kalman filter, though as we will see, on some problems Algorithm 4 has significant advantages.

**Algorithm 4.**

- (1) Begin with  $M$  weighted samples  $\{(X_j(t_{n-1}), W_j(t_{n-1}))\}_{j=1}^M$  approximating  $p(x_{n-1} | h_1, \dots, h_{n-1})$ .
- (2) Determine the sample mean  $\hat{m}_{n-1}$  and covariance  $\hat{\Sigma}_{n-1}$  of the  $\{X_j(t_{n-1})\}_{j=1}^M$ .
- (3) Find the solution  $\hat{\varphi}$  of the optimization problem

$$\inf_{\varphi} \left\{ I_{t_{n-1}, t_n}(\varphi) + \frac{1}{2} |\hat{\Sigma}_{n-1}^{-1/2} (\varphi(t_{n-1}) - \hat{m}_{n-1})|^2 + g(h_n, \varphi(t_n)) \right\}$$

- (4) For each  $j$ , generate an independent sample  $\hat{X}_j$  of the solution to

$$\dot{\hat{X}}_j(t) = b(\hat{X}_j(t)) + \sigma(\hat{X}_j(t)) v(t) + \sqrt{\epsilon} \sigma(\hat{X}_j(t)) \dot{B}(t), \quad t \in [t_{n-1}, t_n]$$

where  $\hat{X}_j(t_{n-1})$  is a Gaussian random vector with mean  $\hat{\varphi}(t_{n-1})$  and covariance  $\hat{\Sigma}_{n-1}$ . Here

$$v(t) = \sigma^{-1}(\hat{\varphi}(t)) \left( \dot{\hat{\varphi}}(t) - b(\hat{\varphi}(t)) \right).$$

(5) Compute the mean  $\hat{m}_n$  and covariance  $\hat{\Sigma}_n$  by

$$\hat{m}_n = \frac{\sum_{j=1}^M \hat{X}_j(t_n) W_j(t_n)}{\sum_{j=1}^M W_j(t_n)} \quad \text{and} \quad \hat{\Sigma}_n = \frac{\sum_{j=1}^M (\hat{X}_j(t_n) - \hat{m}_n)(\hat{X}_j(t_n) - \hat{m}_n)^T W_j(t_n)}{\sum_{j=1}^M W_j(t_n)}$$

where

$$W_j(t_n) = e^{-\frac{1}{2}(\hat{X}_j(t_{n-1}) - \hat{m}_{n-1})^T \hat{\Sigma}_{n-1}^{-1}(\hat{X}_j(t_{n-1}) - \hat{m}_{n-1}) + \frac{1}{2}(\hat{X}_j(t_{n-1}) - \hat{\varphi}(t_{n-1}))^T \hat{\Sigma}_{n-1}^{-1}(\hat{X}_j(t_{n-1}) - \hat{\varphi}(t_{n-1}))} \\ \times e^{-\frac{1}{\epsilon} g(h_n, \hat{X}_j(t_n))} Z_j$$

and

$$Z_j = e^{-\frac{1}{\sqrt{\epsilon}} \int_{t_{n-1}}^{t_n} (v(s), dB_j(s)) - \frac{1}{2\epsilon} \int_{t_{n-1}}^{t_n} |v(s)|^2 ds}$$

Notice that Algorithm 4 only requires the solution of one optimization problem per observation time. In our tests the cost of Step iii is only about 10 times the cost of the evolution of a single trajectory in Step iv, i.e. the cost of running Algorithm 4 is comparable to the cost of running Algorithm 2 with 10 additional particles. Thus it seems that this algorithm is only marginally more expensive than the standard particle filter. The reader should appreciate that while this algorithm does assume that the posterior is Gaussian, it does not assume that the predictive density is Gaussian. This is the key to its advantage over the ensemble Kalman filter. For some problems this algorithm may benefit from the addition of a particle clustering step and a separate solution of the optimization problem in Step iii for each cluster (with different mean and covariance for each cluster). Finally we mention that while Algorithm 3 employs a resampling step, one can easily imagine variants that do not. For example, one can modify these algorithms to incorporate the sample transformations in [4].

## 5. A SIMPLE MODEL OF THE KUROSHIO

The filtering algorithms described in the previous sections will be tested on a stochastic perturbation of the barotropic vorticity equation introduced by [5] to model the Kuroshio current:

$$(28) \quad \partial_t X + \frac{\partial}{\partial x}(uX) + \frac{\partial}{\partial y}(vX) + f \left( \frac{f_x}{f} - \frac{r_x}{r} \right) u + f \left( \frac{f_y}{f} - \frac{r_y}{r} \right) v = \nu \Delta X + \sigma \eta$$

Here  $X(t, x, y)$  is the vorticity,  $r(x, y)$  is the water depth,  $f(x, y)$  is the Coriolis parameter,  $\nu$  is the horizontal eddy diffusivity,  $(u, v)$  are the velocities in the  $x$  and  $y$  directions, respectively, and  $\eta$  is a space-time white noise whose amplitude is controlled by  $\sigma$ .

In this model, as in Chao's original model, the coordinates  $x, y$  are rotated 20 deg counter-clockwise from North-South, and (28) is solved in the domain  $D$  shown in Fig. 3. The viscosity and noise parameters are set to

$$\nu = 8 \times 10^{-4} \quad \text{and} \quad \sigma = 6 \times 10^{-13}$$

The Coriolis parameter is given by

$$f = f_0 + f_x x + f_y y$$

where

$$f_x = \beta \sin(20^\circ) \quad \text{and} \quad f_y = \beta \cos(20^\circ)$$

and  $\beta$  and  $f_0$  are given by  $\beta = 2 \times 10^{-7}$  and  $f_0 = 7 \times 10^{-5}$ . Unless otherwise specified, all distances are measured in kilometers and time is measured in seconds. The function  $r(x, y)$  is the water depth and away from the two bumps that model the Izu Ridge, it is set to the fixed value of 1 kilometer. The northern bump is defined by

$$r_N(x, y) = 0.5 \cos \left( \frac{\pi}{2} \sqrt{\frac{(x - 1410)^2 + (y - 1020)^2}{90}} \right)$$

for

$$\sqrt{(x - 1410)^2 + (y - 1020)^2} \leq 90$$

and the southern bump is defined by

$$r_S(x, y) = 0.5 \cos \left( \frac{\pi}{4} \sqrt{\left( \frac{x'}{120} \right)^2 + \left( \frac{y'}{90} \right)^2} \right)$$

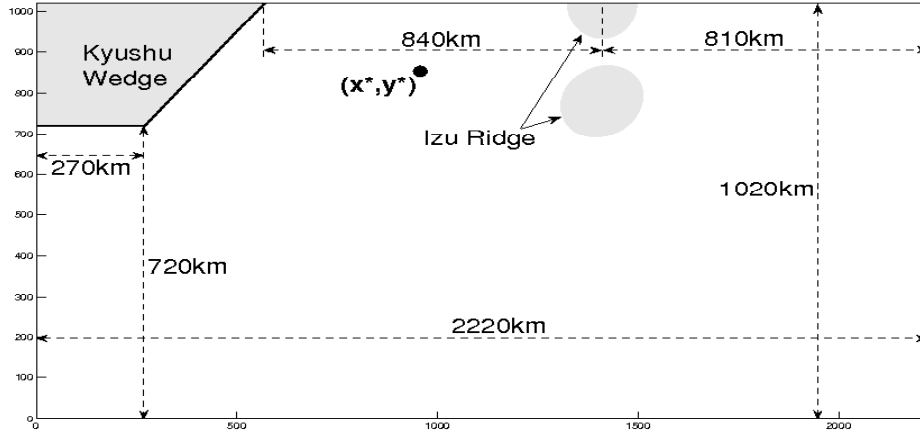


FIGURE 3. Model geometry.

for

$$\sqrt{\left(\frac{x'}{120}\right)^2 + \left(\frac{y'}{90}\right)^2} \leq 1$$

where

$$x' = \frac{(x - 1410) + (y - 780)}{\sqrt{2}}$$

and

$$y' = \frac{(x - 1410) - (y - 780)}{\sqrt{2}}.$$

The horizontal velocities  $u$  and  $v$  satisfy

$$(ru, rv) = (-\psi_y, \psi_x)$$

where the volume transport streamfunction  $\psi$  solves

$$X = \frac{\partial}{\partial x} \left( \frac{1}{r} \psi_x \right) + \frac{\partial}{\partial y} \left( \frac{1}{r} \psi_y \right)$$

The boundary conditions are

<i>I</i>	$\psi = 0,$	$X = 0,$	at $y = 0,$
<i>II</i>	$\psi = -33 Sv,$	$\psi_n = 0,$	along the northern boundary,
<i>III</i>	$\psi_x = 0,$	$\psi_{xx} = 0,$	at $x = 0,$
<i>IX</i>	$\psi = K(y),$	$\psi_{xx} = 0,$	at $x = 2220$

where

$$K(y) = 0 \quad \text{for} \quad y \leq 870$$

and

$$K(y) = -33 \frac{y - 870}{150} Sv \quad \text{for} \quad y > 870.$$

In the above formulas ‘ $Sv$ ’ stands for ‘Sverdrup’ and 1  $Sv$  represents a volume transport of  $10^{-3} km^3 s^{-1}$ .

While (28) is far from a state of the art geophysical representation of the Kuroshio current, it is able to reproduce the large and small meanders of the current: in the deterministic model, these states are basins of attraction of the system forced by the Kyushu wedge and Izu ridge (see Figure 3). Both meanders coexist only for certain inflow volume conditions. For the deterministic model ( $\sigma = 0$ ) Chao demonstrated that it is possible to observe the transition

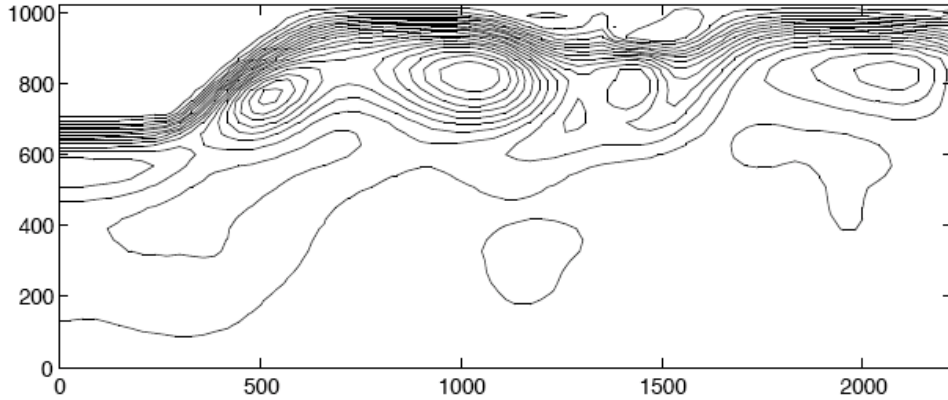


FIGURE 4. Small meander state of the model, (28). The domain is as depicted in Figure 3.

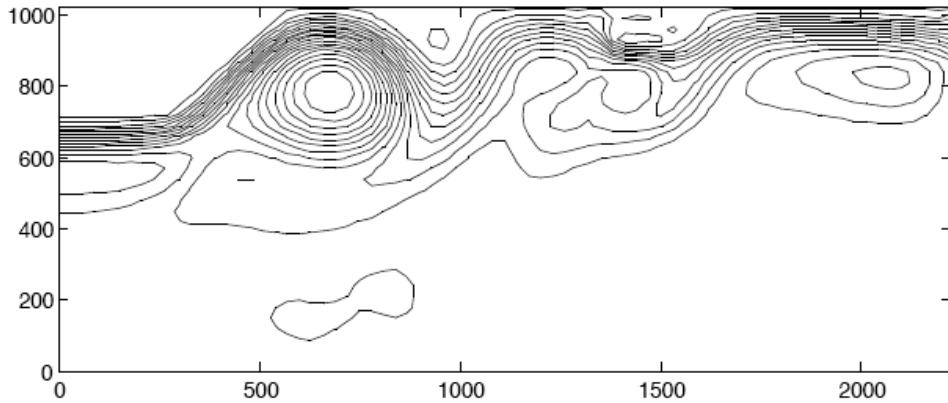


FIGURE 5. Large meander state of the model, (28). The domain is as depicted in Figure 3.

between meanders by varying the inflow condition. The stochastic modification (28) of Chao's model was introduced by one of the authors in [31] and [32] where it was used to test a path sampling based filtering algorithm.

In our calculations, we discretized (28) using a uniform 30 kilometer grid exactly as described in [32, 31] and in Appendix A. The 2516 dimensional discrete time process so obtained (which we also denote by  $X$ ) exhibits two meta-stable states that are qualitatively similar to the small and large meanders of the actual Kuroshio current. Figures 4 and 5 show typical states in both of these meanders. They were found by varying the northern boundary condition as in [5]. The noise parameter in (28) ( $\sigma$ ) was set to 0 for the purposes of generating Figures 4 and 5.

Let  $(x^*, y^*)$  denote the point in  $D$  that is 990km from the western boundary and 860km from the southern boundary. This point is pictured in Figure 3. The bimodality of the system is evident in Figure 6 which shows a long trajectory of the system projected onto the variable  $\psi(x^*, y^*)$ . The state for which  $\psi(x^*, y^*) \approx 15Sv$  roughly corresponds to the small meander and the state for which  $\psi(x^*, y^*) \approx -20Sv$  roughly corresponds to the large meander. As can also be seen in Figure 6 the discrete stochastic system tends to remain in each of its meanders for roughly 10 years. Transitions between the two meanders usually occur in a time span of a few months (though we again caution that this model is far from state of the art).

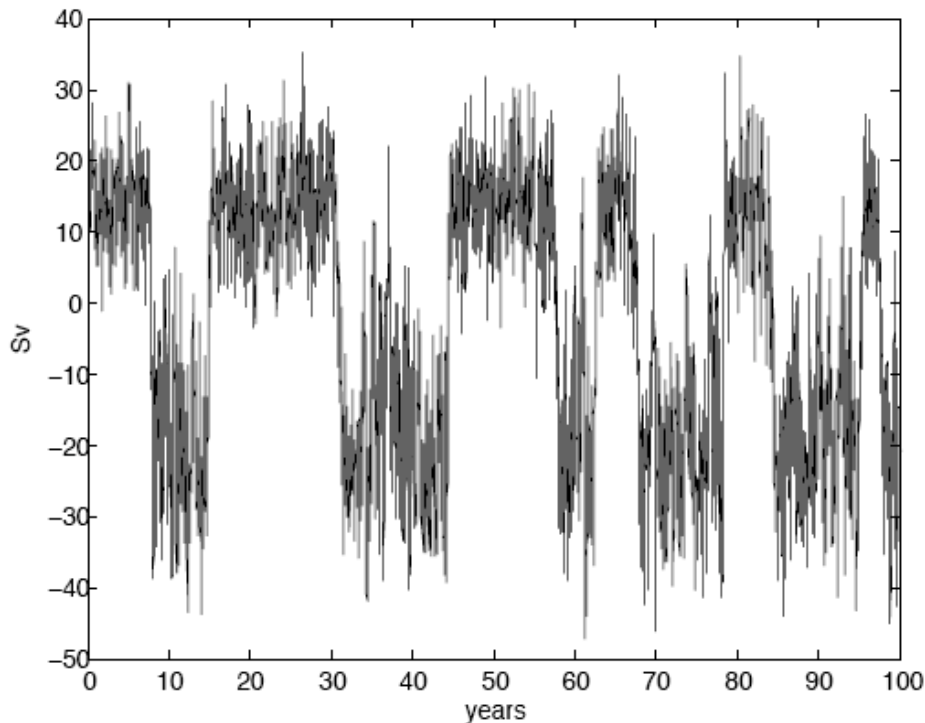


FIGURE 6. Time series of approximation to  $\psi(x^*, y^*)$  where  $(x^*, y^*)$  denotes the point in  $D$  that is  $990km$  from the western boundary and  $860km$  from the southern boundary. Notice the transitions between a metastable state near  $15Sv$  and one near  $-20Sv$ .

Conditioned on the state  $X(t_n)$ , the observation at time  $t_n$ ,  $H_n$ , is a Gaussian random variable with mean  $\psi(t_n)_{k^*, m^*}$  and standard deviation 1.92918. Thus the discrete vorticity process  $X$  is observed through the value of the corresponding volume transport process  $\psi(t_n)$  at the single point  $(k^*, m^*)$ . The observation times are separated by 2.63 days.

**5.1. Test results.** Using the setup described in the previous section we perform a simple but revealing test of the ability of the four filters discussed in this paper to track a single transition of the system from one meander to another. All Algorithms begin from a single initial state in the small meander. The observations are plotted in Figures 7 and 9–12, and correspond to a segment of a long simulation of the system in which the system transitions from the small meander to the large meander. We do not add noise to these observations. The resulting estimates produced by each of the four algorithms are displayed in Figure 7. Evidently Algorithms 3 and 4 are able to properly assimilate the change in the underlying state while the particle filter and the ensemble Kalman filter do not perform as well. The ensemble Kalman filter completely misses the transition while the particle filter seems to eventually capture it but remains relatively far from the estimates produced by Algorithms 3 and 4.

While for a large enough number of samples the particle filter would give the correct result, it is important to observe that the results for the ensemble Kalman filter are fully converged. No matter how many particles are used in the ensemble Kalman filter it will not be able to effectively track the transition. This is because, as discussed earlier, the ensemble Kalman filter uses an extremely poor approximation of the tail of the predictive density, resulting in an estimate that is nearly arbitrary in problems highly sensitive to tail characteristics. The particular transition that we have used to define the observations is more rapid than most of the transitions that we observed in our long simulation of the system. On a slower transition the particle filter will show improved results. The ensemble Kalman filter performed poorly in all the cases that we examined. In our implementations of the ensemble Kalman filter and Algorithm 4 we make the assumption that the posterior covariance matrix ( $\hat{\Sigma}_n$ ) is diagonal though we do not assume that the Kalman gain matrix is diagonal in the calculation of  $\hat{m}_n$  in the ensemble Kalman filter (through an application

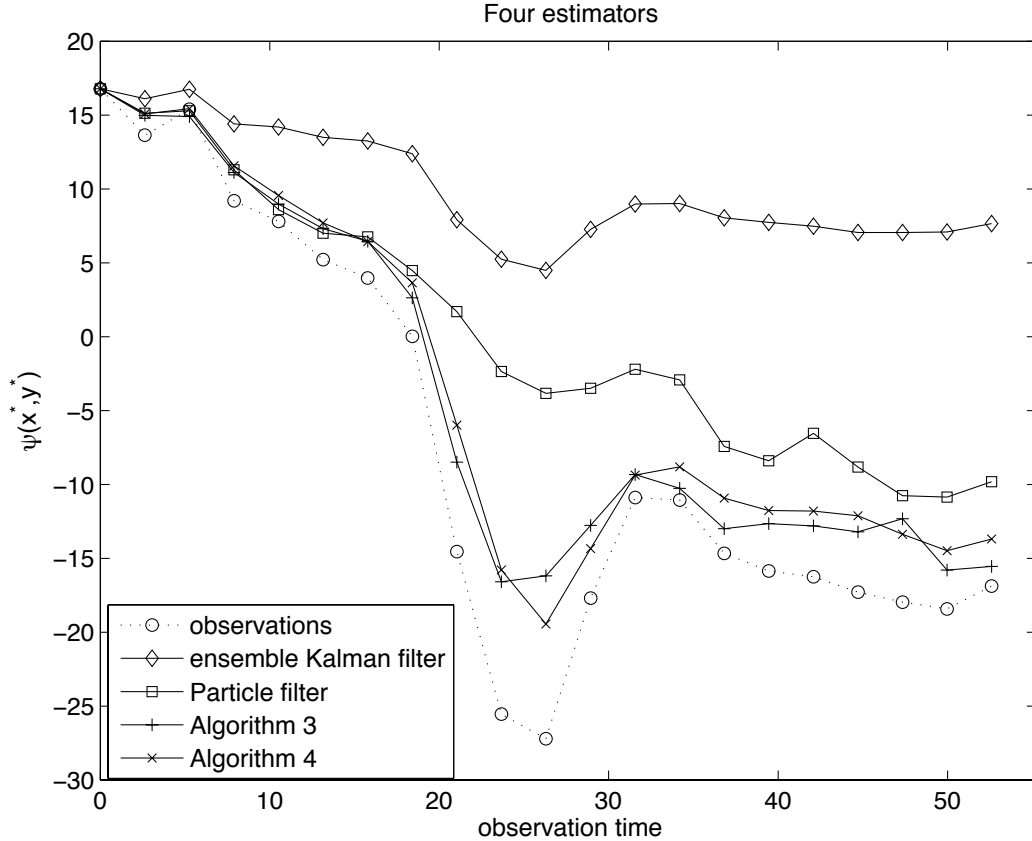


FIGURE 7. Trajectory of estimate of  $\psi(x^*, y^*)$  given observation for the four algorithms outlined in this paper.  $(x^*, y^*)$  is the point in  $D$  that is 990m from the western boundary and 860m from the southern boundary. The particle filter, the ensemble Kalman filter, and Algorithm 4 are all run with 100 particles while Algorithm 3 is run with 10 particles. The estimates produced by Algorithms 3 and 4 track the signal more closely than the ensemble Kalman filter and the particle filter.

of the Sherman-Morrison formula). In the ensemble Kalman filter we also assume that the predictive covariance matrix ( $\Sigma_n$ ) is diagonal.

Only two of the schemes tested (Algorithm 3 and the particle filter) are statistically consistent in the sense that they exactly reproduce the posterior mean given a large enough sample size. For these two schemes we give the values of  $R$  (defined in (8) and (14), respectively) in Figure 8. Recall that by dividing the number of samples by  $R - 1$  one obtains the so-called effective sample size, a rule of thumb giving the number of unweighted samples that would be equivalent (in terms of statistical accuracy) to an ensemble of weighted samples (see for example [8]). The results suggest that the ensemble generated by Algorithm 3 is of much higher statistical quality than the ensemble generated by the particle filter in the sense that to achieve the same accuracy as Algorithm 3 the particle filter would require as many as 100 times the number of samples. We do not compare similar statistics for the two more approximate schemes (the ensemble Kalman filter and Algorithm 4).

We run the particle filter and the ensemble Kalman filter with 100 particles each ( $M = 100$ ). Algorithm 3 is run with only 10 particles ( $M = 10$ ). Algorithm 4 is run with 100 particles ( $M = 100$ ). In Algorithm 3 we set  $\tau = 0.263$  days (see expression (27)). With these choices, the particle filter, the ensemble Kalman filter, and Algorithm 4 have roughly equal cost. Algorithm 3 is several times more expensive than the others. The optimizations in Algorithm 3 and 4 typically converge to an acceptable level of accuracy in a handful of iterations (using a total of 10 Jacobian multiplications or less). For more details on how these optimizations are carried out see Appendix B.

In Figures 9–12 we represent the empirical densities produced by the four algorithms. In each figure a vertical line is drawn at each sample value of  $\psi(x^*, y^*)$  at every observation time. The height of each line is the weight of that sample.

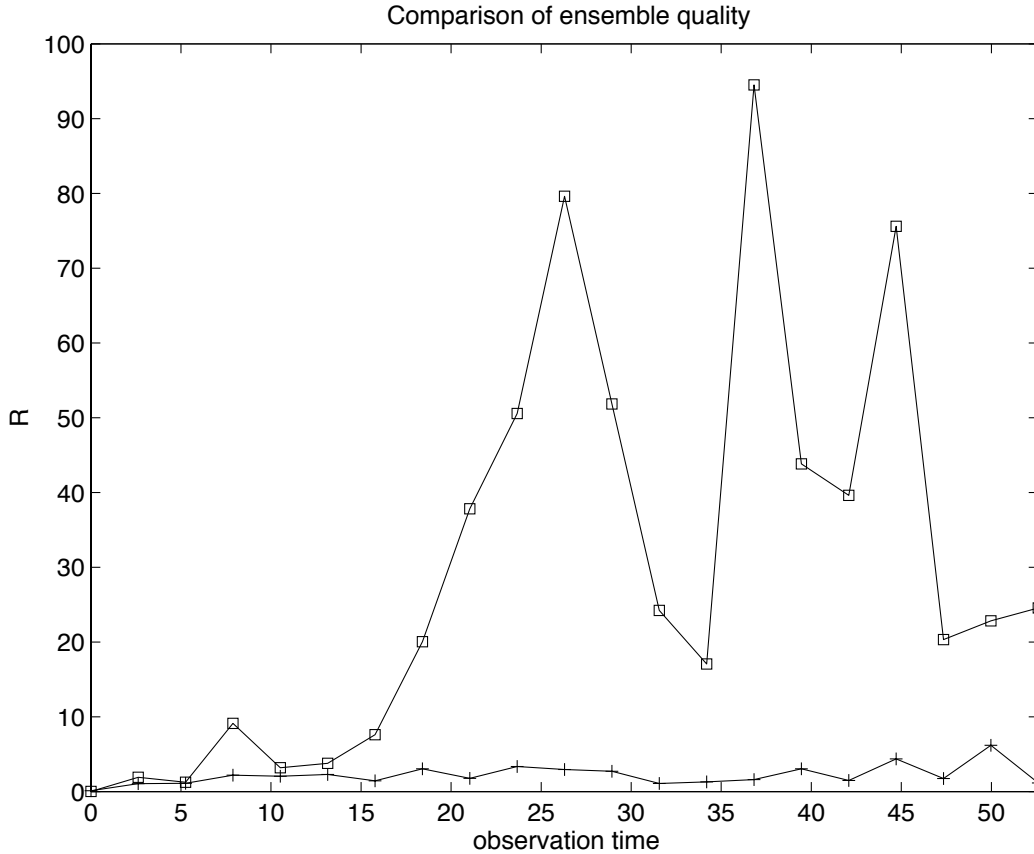


FIGURE 8. The values of  $R$  defined in equations (8) (for the particle filter with 100 particles) and (14) (for Algorithm 3 with 10 particles). The effective sample size (see for example [8]) for the two algorithms is found by dividing the number of particles by  $R - 1$ . We plot the  $R$  values only for the two statistically consistent schemes (Algorithm 3 and the particle filter), that is the schemes that we know to converge to the correct density as the number of samples is increased. This plot suggests that the ensemble generated by Algorithm 3 is of much higher statistical quality than the ensemble generated by the particle filter in the sense that to achieve the same accuracy as Algorithm 3 the particle filter would require as many as 100 times the number of samples. It is not a meaningful statistic for approximate schemes such as Algorithm 4 or the ensemble Kalman filter.

One can clearly see that the ensembles generated by the particle filter are dominated by a single particle at many of the observation times while the other schemes produce more regular weights. Again we can see that the ensembles generated by the particle filter and the ensemble Kalman filter are concentrated much farther from the observations than the ensembles generated by Algorithms 3 and 4. Of course proximity to the observation is not a reliable measure of success in filtering (proximity to the posterior density is our goal). However, given that both Algorithms 3 and 4 agree, we conclude that they are accurate.

## 6. CONCLUSION

We have suggested that the failure of standard filtering algorithms such as ensemble Kalman filters and particle filters on certain problems can be easily understood and analyzed in a low noise regime. As a first attempt at overcoming these issues we propose two schemes based on rare event simulation tools. The field of rare event simulation has seen explosive growth over the last decade or so and our investigation here is far from an exhaustive study of the potential utility of rare event tools within data assimilation. However, our results do strongly indicate that more investigation in this direction is warranted.



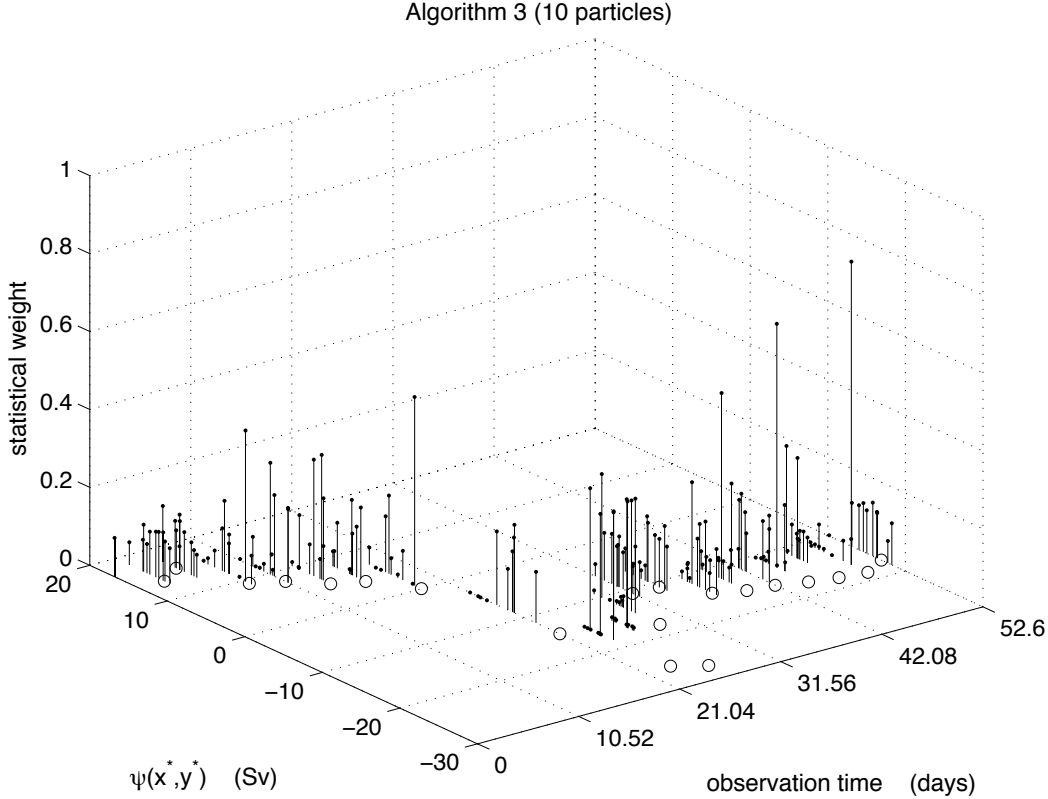


FIGURE 9. Plot of the values of  $\psi(x^*, y^*)$  corresponding to the samples  $\hat{X}_j$  generated in Step ii of Algorithm 3 (with 10 particles) at each observation time. The  $z$ -coordinate of each point is the value of the weights (normalized) computed in Step iii of the algorithm. Most the 10 particles have weight comparable to the mean weight (in this case 0.1) and the particle values of  $\psi(x^*, y^*)$  are clustered near the observation.

In the context of the Kuroshio where standard methods fail, our new methods inspired by rare event simulation techniques are very effective. Of course, the application of these methods is not limited to the study of the Kuroshio current. Even restricting our attention to geophysics, one can imagine important applications such as the prediction of short and medium term extreme geophysical events like tsunamis, hurricanes, and drought, as well as paleoclimate data assimilation. We also remark that the hybrid nature of our schemes suggest that they could be combined with existing large scale data assimilation code employed in a black box fashion to design new robust algorithms.

In our numerical test we have chosen to focus on a system with an obvious, interesting tail feature (the meander transition). While problems of this kind provide stark evidence that current filtering practice can be inadequate, it is important to point out that the same failures can occur on problems with more mundane tail behaviors. Indeed, over long periods of time one can expect nearly any underlying (“hidden”) process to undergo rare excursions. In exactly the way that we have demonstrated, these excursions will cause standard methods to loose track of the signal.

Finally we would like to point out that the methods proposed here are related to schemes proposed in [7, 6] and called “implicit sampling” methods. In those schemes one attempts to construct a map taking an easily sampled random variable (usually a multidimensional Gaussian) to a random variable distributed according to the posterior density. The function  $v^\epsilon$  defined in (16) is an exact solution to this problem. It can be used to map the trajectory of a Brownian motion (an easily sampled random variable) to a random variable (the corresponding  $\hat{X}(T)$ ) drawn exactly from the posterior density. In the low noise regime that we focus on, good statistical behavior does not require that the mapping be exact. For example, the theoretical results in [29] indicate that an asymptotic (in the small noise limit) approximation of  $v^\epsilon$  ( $v^0$  in (23)) can yield strikingly good error behavior. The importance sampling schemes at the core of Algorithms 3 and 4 are based on further approximations of  $v^\epsilon$  and perform extremely well in our tests.

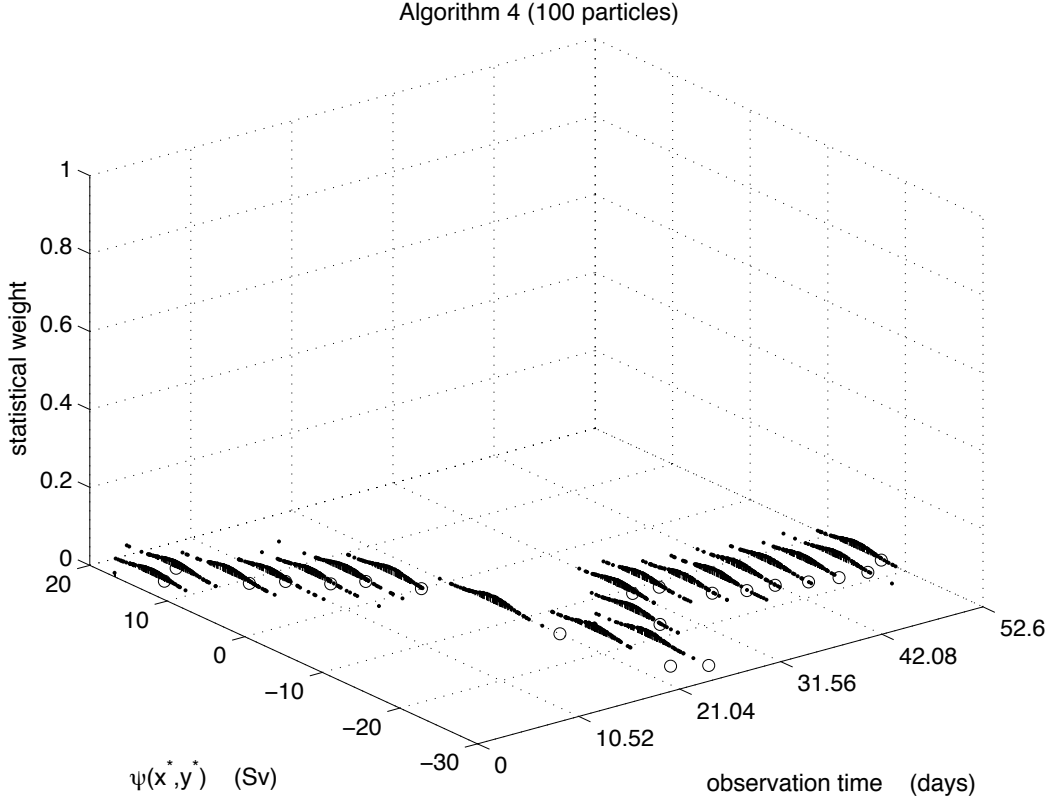


FIGURE 10. Plot of the values of  $\psi(x^*, y^*)$  corresponding to the samples  $\hat{X}_j$  generated in Step iv of Algorithm 4 (with 100 particles) at each observation time. The  $z$ -coordinate of each point is the value of the weights (normalized) computed in Step v of the algorithm. All 100 particles have weight comparable to the mean weight (in this case 0.01) and the particle values of  $\psi(x^*, y^*)$  are clustered near the observation.

#### ACKNOWLEDGMENTS

We would like to thank Professors Dorian Abbot, Alexandre Chorin, and Juan Restrepo for helpful conversations. We would also like to thank Professor Chorin for suggesting the Kuroshio current to JW as an interesting test system. The efforts of EVE were supported by NSF through award DMS-0708140, by DOE through award DE-SC0002618, and by ONR through award N00014-11-1-0345. The efforts of JW were supported by NSF through award DMS-1109731.

#### APPENDIX A: DISCRETIZED KUROSHIO MODEL

Let  $\Delta_x = 30km$  denote the spatial mesh size which is the same in both the  $x$  and  $y$  directions. For any function  $g$  on  $D$  define

$$g_{k+\alpha_x, l+\alpha_y} = g((k + \alpha_x)\Delta_x, (l + \alpha_y)\Delta_x)$$

for  $\alpha_x, \alpha_y \in [-1, 1]$ . Define the operators

$$\begin{aligned} \delta_x g &= \frac{g_{k+1/2, m} - g_{k-1/2, m}}{\Delta_x}, & \delta_y g &= \frac{g_{k, m+1/2} - g_{k, m-1/2}}{\Delta_x}, \\ \mu_x g &= \frac{g_{k+1/2, m} + g_{k-1/2, m}}{2}, & \mu_y g &= \frac{g_{k, m+1/2} + g_{k, m-1/2}}{2}, \\ D_x^0 &= \mu_x \delta_x, & D_y^0 &= \mu_y \delta_y, \end{aligned}$$

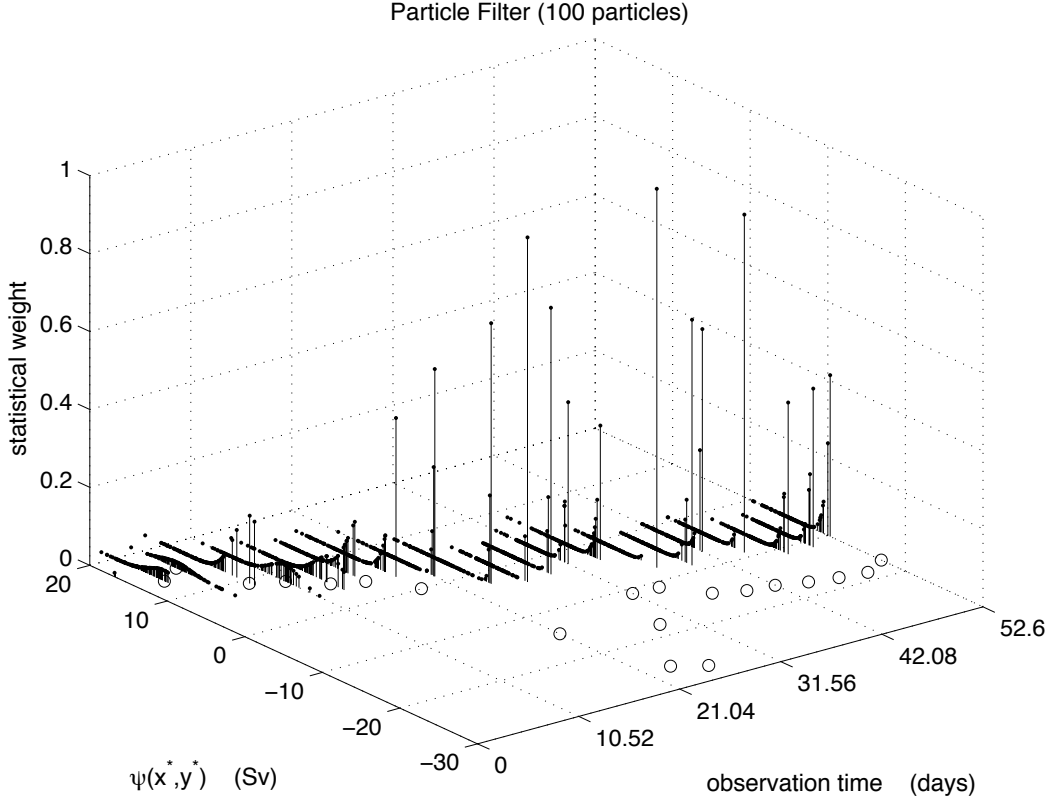


FIGURE 11. Plot of the values of  $\psi(x^*, y^*)$  corresponding to the samples  $\hat{X}_j$  generated in Step ii of the standard particle filter (with 100 particles) at each observation time. The  $z$ -coordinate of each point is the value of the weights (normalized) computed in Step iii of the algorithm. At several steps there is only one particle with appreciable weight and that particle's value of  $\psi(x^*, y^*)$  is far from the observations compared to the corresponding values generated by Algorithms 3 and 4.

and

$$(29) \quad L^0 = \delta_x \left( \frac{\delta_x}{h} \right) + \delta_y \left( \frac{\delta_y}{h} \right).$$

First, (28) is discretized in space using a simple centered difference scheme which involves only values of  $X$  at points  $(k\Delta_x, m\Delta_x)$ . After replacing  $X$  by its restriction to these points the system becomes a set of ordinary stochastic differential equations,

$$(30) \quad \dot{X}_{k,m}(t) = F_{k,m}(X(t)) + \frac{1}{\Delta_x} \sigma \dot{B}_{k,m}(t)$$

where

$$(31) \quad F_{k,m}(X(t)) = -D_x^0(u_{k,j}X_{k,j}) - D_y^0(v_{k,m}X_{k,m}) \\ - f_{k,m} \left( \frac{f_x}{f_{k,m}} + D_x^0 \left( \frac{1}{h} \right) \right) u_{k,m} - f_{k,m} \left( \frac{f_y}{f_{k,m}} + D_y^0 \left( \frac{1}{h} \right) \right) v_{k,m} \\ + \nu (\delta_x \delta_x + \delta_y \delta_y) X_{k,m}$$

where  $\psi$  solves

$$(32) \quad L^0 \psi = X$$

and

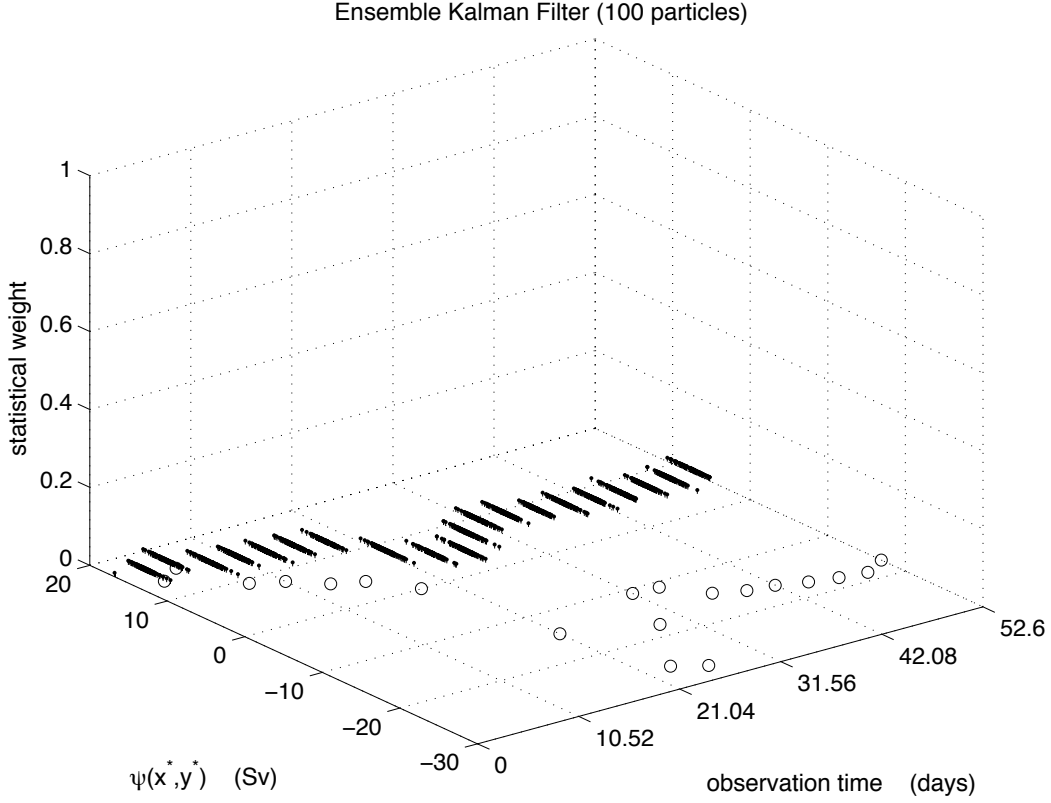


FIGURE 12. Plot of the values of  $\psi(x^*, y^*)$  corresponding to the samples  $\hat{X}_j$  generated in Step ii of the ensemble Kalman filter (with 100 particles) at each observation time. The  $z$ -coordinate of each point is 0.01 (the weights in this scheme are constant). The particle values of  $\psi(x^*, y^*)$  are far from the observations compared to the corresponding values generated by Algorithms 3 and 4.

$$u_{k,m} = -\frac{D_y^0 \psi_{k,m}}{h}, \quad v_{k,m} = \frac{D_x^0 \psi_{k,m}}{h}.$$

The  $B_{k,m}$  are independent Brownian motions. Consistent with the previous sections,  $X(t_n)$  denotes the solution of (33) at the time of  $l$ th observation.

These stochastic ordinary differential equations cannot be solved explicitly and therefore require numerical solution. Here the spatially discretized system (30) is discretized in time as

$$(33) \quad X_{k,m}((n+1)\Delta) = X_{k,m}(n\Delta) + (F_{k,m}(\check{X}_{k,m}) + F_{k,m}(X_{k,m}(n\Delta))) \frac{\Delta}{2} + \frac{\sqrt{\Delta}}{\Delta_x} \sigma \eta_{k,m}(n)$$

where

$$\check{X}_{k,m} = X_{k,m}(n\Delta) + F_{k,m}(X_{k,m}(n\Delta)) \Delta + \frac{\sqrt{\Delta}}{\Delta_x} \sigma \eta_{k,m}(n)$$

and now for each  $k$ ,  $m$ , and  $n$ ,  $\eta_{k,m}(n)$  is an independent Gaussian random variable with mean 0 and variance 1. The resulting method is adequate for the relatively low Reynolds number flow considered here. A Crank Nicholson type scheme was not applied to the linear part of the equation because the stiffness of the system is not dominated by the diffusion term at the level of discretization used here.

## APPENDIX B: SOLVING FOR $\hat{\varphi}$

Both Algorithms 3 and 4 require solving an optimization problem at least once at each observation time. As both problems are similar we will focus on the minimization of functionals of the form

$$\int_0^T \frac{1}{2} |\sigma(\varphi(s))^{-1} (\dot{\varphi}(s) - b(\varphi(s)))|^2 ds + g(\varphi(T)).$$

Note that the minimizer of this action solves the ordinary differential equation

$$\dot{\varphi} = b + \sigma \hat{u}$$

where  $u \in L^2([0, T])$  minimizes

$$\int_0^T \frac{1}{2} |u(s)|^2 ds + g(\varphi_u(T)).$$

Because it tends to be well scaled, it is this cost function (after time discretization) that we choose to optimize. The discretization corresponding to the discrete version of the process described in the last appendix is simply

$$(34) \quad \sum_{n=0}^{T/\Delta-1} \frac{1}{2} |u(n)|^2 \Delta + g(\varphi_u(T))$$

where now

$$\varphi_u((n+1)\Delta) = \varphi_u(n\Delta) + \frac{\Delta}{2} (b(\tilde{\varphi}_u) + b(\varphi_u(n\Delta))) + \frac{1}{\Delta_x} \sigma u(n)$$

and

$$\tilde{\varphi}_u = \varphi_u(n\Delta) + b(\varphi_u(n\Delta)) \Delta + \frac{1}{\Delta_x} \sigma u(n).$$

In the minimization of (34) we use the conjugate gradient method (thereby avoiding the formation of any Jacobian matrices) within a trust region framework (see in particular the algorithms on pages 69 and 171 in [24]). A disadvantage of working in the  $u$  variables is that the evaluation of  $\varphi_u(T)$  is a serial operation making the procedure less amenable to parallel implementation. Finally note that in Algorithm 3 requires repeated minimization of function of the form (34) during the generation of each sample trajectory. This can be accelerated by the use of a continuation strategy, using the result of the previous optimization to initiate the next.

## REFERENCES

- [1] F. Alexander, G. Eyink, and J. Restrepo. Accelerated Monte Carlo for optimal estimation of time series. *Journal of Statistical Physics*, 119:1331–1345, 2004.
- [2] A. Apte, C. Jones, and A. Stuart. A bayesian approach to lagrangian data assimilation. *Tellus A*, 60:336–347, 2008.
- [3] M. Bardi and I. Capuzzo-Dolcetta. *Optimal Control and Viscosity Solutions of Hamilton-Jacobi-Bellman Equations*. Birkhauser, 2008.
- [4] P. Bickel and J. Lei. Ensemble filtering for high dimensional nonlinear state space models. preprint.
- [5] S. Chao. Bimodality of the Kuroshio. *J. Phys. Oceanogr.*, 14:92–103, 1984.
- [6] A. Chorin, M. Morzfeld, and X. Tu. Implicit filters for data assimilation. *Comm. Appl. Math. Comp. Sc.*, 5:221–240, 2010.
- [7] A. Chorin and X. Tu. Implicit sampling for particle filters. *Proc. Nat. Acad. Sci.*, 106:17249–17254, 2009.
- [8] N. de Freitas, A. Doucet, and N. Gordon (Eds). *Sequential Monte Carlo Methods in Practice*. Springer, 2005.
- [9] A. Dembo and O. Zeitouni. *Large Deviations Techniques and Applications*. Springer, 1993.
- [10] P. Dupuis and R. S. Ellis. *A Weak Convergence Approach to the Theory of Large Deviations*. Wiley, 1997.
- [11] G. Evensen. The ensemble Kalman filter: theoretical formulation and practical impementation. *Ocean Dynamics*, 53:343–367, 2003.
- [12] W. Fleming and H. Soner. *Controlled Markov Processes and Viscosity Solutions*. Springer, 2006.
- [13] M. Freidlin and A. Wentzell. *Random Perturbations of Dynamical Systems*. Springer, 1984.
- [14] N. Gordon, D. Salmond, and A. Smith. Novel approach to nonlinear non-Gaussian Bayesian state estimation. *IEE Proceedings F*, 51:107 – 113, 1993.
- [15] M. Heymann and E. Vanden-Eijnden. Novel approach to nonlinear non-Gaussian Bayesian state estimation. *Communications on Pure and Applied Mathematics*, 61:1052–1117, 2008.
- [16] B. Hunt, E. Kostelich, and I. Szunyogh. Efficient data assimilation for spatiotemporal chaos: a local ensemble transform kalman filter. *Physica D*, 230:112–126, 2007.
- [17] S. Shreve I. Karatzas. *Brownian Motion and Stochastic Calculus*. Springer, 1991.
- [18] R. Kalman. A new approach to linear filtering and prediction problems. *J. Basic Eng.*, 82:35–45, 1960.
- [19] G. Kitagawa. Monte Carlo filter and smoother for non-gaussian nonlinear state space models. *Journal of Computational and Graphical Statistics*, 5:1–25, 1996.
- [20] K. Law and A. Stuart. Evaluating data assimilation algorithms. submitted.
- [21] J. Lei, P. Bickel, and C. Snyder. Comparison of ensemble kalman filters under non-gaussianity. *Mon. Wea. Rev.*, 138:1293–1306, 2010.

- [22] J. Liu. *Monte Carlo Strategies in Scientific Computing*. Springer, 2002.
- [23] R. Miller, E. Carter, and S. Blue. Data assimilation into nonlinear stochastic models. *Tellus A*, 51:167–194, 1999.
- [24] J. Nocedal and S. Wright. *Numerical Optimization*. Springer, 2006.
- [25] E. Ott, B. Hunt, I. Szunyogh, A. Zimin, E. Kostelich, M. Corazza, E. Kalnay, and D. Patil. A local ensemble kalman filter for atmospheric data assimilation. *Tellus*, 56A:415–428, 2004.
- [26] B. Qiu and W. Miao. Kuroshio path variations south of Japan: bimodality as a self-sustained internal oscillation. *J. Phys. Oceanogr. (2000)*, 30 2124, 30:2124–2137, 2000.
- [27] F. Rabier, H. Jarvinen, E. Klinker, J. Mahfouf, and A. Simmons. The ecmwf operational implementation of four-dimensional variational physics. *Q. J. R. Meteorol. Soc.*, 126:1143–1170, 2000.
- [28] B. Taft. Characteristics of the flow of the Kuroshio south of Japan. In K. Yoshida H. Stommel, editor, *Kuroshio, Physical Aspects of the Japan coast*, pages 165–214. University of Washington Press, 1972.
- [29] E. Vanden-Eijnden and J. Weare. Rare event simulation for small noise diffusions. *Communications on Pure and Applied Mathematics*, accepted.
- [30] S. Varadhan. *Large Deviations and Applications*. Springer, 1985.
- [31] J. Weare. *Bridge path sampling and filtering of stochastic and ordinary differential equations*. PhD thesis, University of California, Berkeley, 2007.
- [32] J. Weare. Particle filtering with path sampling and an application to a bimodal ocean current model. *J. Comp. Phys.*, 228:4312–4331, 2009.
- [33] S. Yang, M. Corazza, A. Carrassi, E. Kalnay, and T. Miyoshi. Comparison of ensemble-based and variational-based data assimilation schemes in a quasi-geostrophic model. *Mon. Wea. Rev.*, 137:693–709, 2009.
- [34] K. Yoshida. On the variations of Kuroshio and cold water mass of Enshu Nada. *Hydrogr. Bull.*, 67:54–57, 1961.